THE RIGAKU JOURNAL
VOL. 19 / NO.1 / 2002

# MODEL PEAK PROFILE FUNCTIONS FOR POWDER DIFFRACTOMETRY AS CONVOLUTIONS WITH INSTRUMENTAL FUNCTIONS

TAKASHI IDA

*Ceramics Research Laboratory, Nagoya Institute of Technology, Asahigaoka, Tajimi 507-0071, Japan*

Model peak profile functions synthesized by convolutions of intrinsic peak profiles with the instrumental functions of powder X-ray diffractometers with conventional and synchrotron Xray sources are presented. The validity of the model functions has been examined by comparing with the experimental peak profiles measured in different conditions. Not only the profiles produced by *a priori* calculation are in good coincidence with the observed profiles, but the intrinsic peak positions are evaluated in advanced precision by applying a profile fitting method. The use of the convoluted model profile functions provides a convenient and reliable way to estimate a lattice constant without use of any standard materials.

## 1. Introduction

Peak profile functions are mathematical models for the shape of the experimental peaks, while powder diffraction patterns are mainly specified by the positions and intensities of diffraction peaks. The experimental peak profiles are modelled by convolutions of intrinsic peak profiles with deformation caused by the instruments used for the measurement. The convoluted model function enables precise extraction of information about the intrinsic peak profiles, including the integrated intensities, locations and widths of the peaks, from experimental diffraction data.

The determination of crystal structure from powder diffraction data is achieved by the following steps: (i) indexing of each peak by hkl, (ii) determination of peak location $2\theta_{hkl}$ or interplanar distance $d_{hkl}$, and (iii) evaluation of integrated intensity $I_{hkl}$. The lattice constants a, b, c, $\alpha$, $\beta$ and $\gamma$ are determined from the series of interplanar distance $\{d_{hkl}\}$, and the structural parameters, i.e. locations and displacement parameters of atoms, are evaluated from sufficient number of intensity data $\{I_{hkl}\}$, which is similar to the structure analysis based on single crystal data. However, the powder diffraction pattern corresponds to a projection of three-dimensional reciprocal lattice onto one-dimension. It is often difficult to obtain accurate $\{I_{hkl}\}$ for closely located powder diffraction peaks which may be heavily overlapped by the projection, because each peak has finite width caused by the spectral width of the beam source and the finite resolution of instruments.

Even if direct extraction of $\{I_{hkl}\}$ is difficult, the crystal structure can be refined by the Rietveld method [1], provided that an appropriate structure model is already known. The most likely structure is obtained by iterative calculation to minimize the deviation of the calculated pattern from the experimental one, the former of which is realized by the sum of the profile functions multiplied by the intensities $\{I_{hkl}\}$ calculated from the trial structure model. The accuracy of the structural parameters determined by the Rietveld method depends on the validity of the profile function as well as the quality of the experimental data. The profile function used in the Rietveld method may include adjustable parameters to fit the experimental profile. However, increased number of adjustable parameters generally causes lower speed of convergence in iterative calculation and also possibility of convergence to fault local minima. Therefore, goodness of a profile function should be judged not only by the fitness to observed profile but also by the number of the required adjustable parameters.

Profile functions are also used for direct evaluation of $\{I_{hkl}\}$, without structural models, from the experimental powder diffraction pattern. In principle, $I_{hkl}$ can directly be obtained by the integration of an experimental peak profile after subtraction of background, but it is difficult to precisely subtract background for peaks with long tail, and additional errors may be caused by finite cut-off of the integral range. Curve fitting method based on an appropriate profile function supplies an accurate and easy way to separate the peak

from background and estimate intrinsic values of integrated intensity, location and width of the peak. Application of appropriate profile functions is particularly important for the purpose of decomposition of overlapped peaks by curve fitting method. Accuracy of decomposition can be improved by good fitness with minimum number of adjustable parameters supplied by an ideal profile function.

An appropriate profile function is not only important for the evaluation of averaged crystal structures as described above. It should be noted that the information about the imperfection of real crystals are intrinsically included in the experimental diffraction peak profiles. In fact, significant peak broadening is observed for small crystallites, when the diameter is smaller than about 100 nm, which enables the estimation of the size of crystallites based on line broadening analysis [2]. However, as the resolution of a real diffractometer is finite, the correction of instrument-induced line broadening is necessary for accurate evaluation of line broadening, when the crystallite is not very small. It means that the improved structure analysis needs the description of the profile parameters explicitly related to the geometry of the instrument.

In this article, the mathematical models of the instrumental functions and the model peak profile functions for (1) the most commonly used diffractometers with focal (Bragg-Brentano) geometry and (2) a high-resolution synchrotron diffractometer attached with crystal analyzer.The results of experimental examination on the validity of the models are also presented.

## 2. Fundamental-parameters Approach

The fundamental-parameters approach, proposed by Cheary et al. [3], is an attempt to express the experimental powder diffraction peak in terms of fundamental parameters with explicit physical meanings, such as spectroscopic parameters of the beam source, geometry of the optical components, and the size and absorption coefficients of the specimens. When the powder sample is well crystallized and not too small in size, the profile function defined by the fundamental-parameters method does not include any adjustable parameters.

The diffraction peak profile function P(x) is expressed by

$$P(x) = p \otimes w_1 \otimes w_2 \otimes w_3 \ldots w_n \qquad (2.1)$$

where x means the diffraction angle in the angle-dispersive measurement or the photon energy in the energy-dispersive measurement; p(x) is the spectroscopic profile of the beam source, and $w_i$ (i= 1,...,n) denotes the aberration caused by the instruments; the symbol $\otimes$ means the convolution defined by

$$f \otimes g \equiv \int_{-\infty}^{\infty} f(x-y)g(y)dy \qquad (2.2)$$

If it is necessary to include sample-induced peak broadenings such as size broadening, those effects can be taken into account as further convolution with appropriate model functions.

Generally, there are three methods to calculate the convolutions: (1) use of analytical solution or approximate solution, (2) numerical integration, and (3) Fourier transform. As any of those calculations often consume considerable time for computing, it is practically important to improve the efficiency of calculation by applying appropriate algorithms.

Recently, the author has developed an efficient algorithm for evaluation of convolutions based on numerical integral, and shown that it satisfactorily works in profile fitting to isolated peaks [4, 5]. The method needs explicit formula of approximated primitive function of the target model function to be convoluted. Following the method, an accurate and smooth model profile function can be systematically synthesized by convolution without theoretical ambiguity.

## 3. Profile Function for Diffractometers with Focal Geometry

### 3.1. Model Function

In this section, the models of spectroscopic profile and the instrumental aberration functions for a commonly used diffractometer with focal (Bragg-Brentano type) geometry (Fig. 1) and Cu Kα X-ray source are described.

#### *3.1.1. Spectroscopic Profile of Cu Kα Source*

The spectroscopic profile of Cu Kα X-ray source has been approximated by the weighted sum of five Lorentzian (Cauchy distribution) functions by Cheary et al. [3], while it has been analyzed with four Lorentzian functions in a more recent literature [4]. Practically, the approxima-

tion by the sum of two Lorentzian functions seems to be sufficient [7], which is given by

$$p(x)=\sum_{i=1}^{2} f_i p_L(x;x_i,\gamma_i) \tag{3.1}$$

$$p_L(x;x_0,\gamma_L)=\frac{1}{\pi\gamma_L}\left[1+\left(\frac{x-x_0}{\gamma_L}\right)^2\right]^{-1} \tag{3.2}$$

$$x_2=2\arcsin\frac{\lambda_2\sin(x_1/2)}{\lambda_1} \tag{3.3}$$

$$\gamma_i=\frac{(\Delta\lambda)_i}{\lambda_i}\tan(x_i/2) \tag{3.4}$$

where $f_i$, $\lambda_i$, $(\Delta\lambda)_i$ are the intensity, wavelength and the full width at half maximum (FWHM) of the Kα; peak, with typical values of $f_1$=2/3, f2=1/3; $\lambda_1$=1.5405981 Å, λ2=1.54443 Å; $(\Delta\lambda)_1$ = 0.00058 Å, $(\Delta\lambda)_2$=0.00077 Å [8].

Although the approximation for the spectroscopic profile of the X-ray source by Lorentzian functions is naturally derived from a linear response theory for resonant absorption/emission, it seems that no decisive parameters for the real Cu Kα radiation have been available. Furthermore, effective values of those parameters may be varied depending on the use of monochromator or a pulse-height analyzer.

*3.1.2. Fundamental Resolution of Diffractometer*

As shown in Fig. 1, the line focus is used as the X-ray source, while a receiving slit is located at the other focal point. Even though the X-ray source has finite width along the equatorial direction, it is usually negligible because the width of the receiving slit is wider than the effective width of the X-ray source. The fundamental resolution of the instrument is approximated by the ratio of the receiving slit $W_R$ and the goniometer radius R. It is assumed that the effect of the finite resolution of the instrument on the diffraction profile is represented by the following Gaussian (normal distribution) function:

$$W_R(x;\gamma_R)=\frac{1}{\sqrt{\pi}\gamma_R}\exp\left[-\left(\frac{x}{\gamma_R}\right)^2\right] \tag{3.5}$$

$$\gamma_R=\frac{\arctan(W_R/R)}{2\sqrt{\ln 2}} \tag{3.6}$$

The Voigt function is defined by the convolution of the Lorentzian and Gaussian functions. As it is quite common that the energy dispersion in the resonant absorption is described by the Lorentian function, as well as the spectroscopic effects of the optics can be approximated by the Gaussian function, the Voigt function is a very important function in the field of spectroscopy, and has already been studied in detail [9]. A reliable algorithm for evaluation of the Voigt profile proposed by Poppe & Weijers, by which the partial derivatives can also be evaluated, is available [10].

The pseudo-Voigt function is the approximation for the Voigt function with the weighted sum of the Lorentzian and Gaussian functions. Wertheim has reported that the deviation of the optimized pseudo-Voigt function from the Voigt function is at most 0.77% relative to the peak height, and it is convenient for rapid computation [11]. However, it should be noted that a frequently used formula for the pseudo-Voigt function, further approximated by Thompson *et al.* [12], shows the maximum deviation of 1.2%, and may cause considerable errors in estimation of parameters.

Recently, the authors have proposed an extended formula of the pseudo-Voigt function obtained by addition of two other functions with intermediate shape between the Lorentzian and Gaussian functions [13]. The extended formula of the pseudo-Voigt function typically needs 2.5-times longer computation time as compared with the formula proposed by Thompson *et al.,* but the deviation from the Voigt function becomes less than 1/10.

*3.1.3. Axial (Vertical) Divergence Effect*

The experimental diffraction peaks generally show asymmetric profiles, with longer tail in the lower side for the low-angle diffractions. This phenomenon is mainly ascribable to the diver-

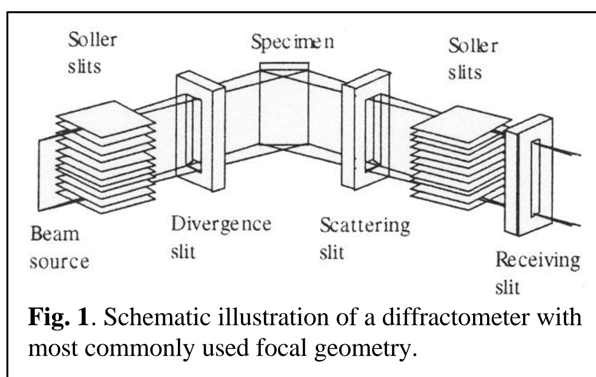


**Fig. 1**. Schematic illustration of a diffractometer with most commonly used focal geometry.

gence of the source and/or diffracted beam along the rotation axis of the goniometer, which is known as the axial or vertical divergence effect.

As shown in Fig. 1, a couple of Soller slits are usually located on both source and diffracted beam sides of a diffractometer. Soller slits are the array of thin metal foils, and the axial beam divergence is limited by the angle determined by the ratio of the separation to the length of the foils. The angular dispersion of the beam intensity limited by the Soller slits shows maximum at the direction of the beam parallel to the equatorial plane, and decrease by deviation of the beam. The author has revealed an analytical expression of the aberration function that mathematically describes the deformation of diffraction profiles caused by the axial divergence limited by the Soller slits [14].

When the angular dispersion along the axial direction obeys the Gaussian distribution with FWHM of $\Phi_v$, the axial-divergence aberration function is given by

$$W_v(z;\gamma_v,t)=\frac{2}{\pi\gamma_v}\exp\left[\left(t-\frac{1}{t}\right)\frac{z}{\gamma_v}\right]K_0\left[\left(t+\frac{1}{t}\right)\frac{|z|}{\gamma_v}\right] \tag{3.7}$$

where, $\gamma_v=\Phi^2_v/4\ln 2$, $t=\tan\theta_0$ for the diffraction angle $2\theta_0$ and $K_0(x)$ is the modified Bessel function of the second kind. The Bessel function is often implemented in computing systems, and reliable numerical routines written in FORTRAN and C-language are available [15]. Note that the formula given by Eq. (3.7) is normalized for any values of $\gamma_v$ and t.

Figure 2 shows the dependence of the shape of the axial-divergence aberration function upon the diffraction angle. When the diffraction angle is just 90° (t=1), the function shows symmetric shape with singularity at $z \to 0$, but has finite width, which is clearly different from the Dirac delta function. The lower-angle tail of the function increases and the higher-angle tail decreases for the lower diffraction angle (t<1), while an opposite change in shape is shown for the higher diffraction angle (t>1).

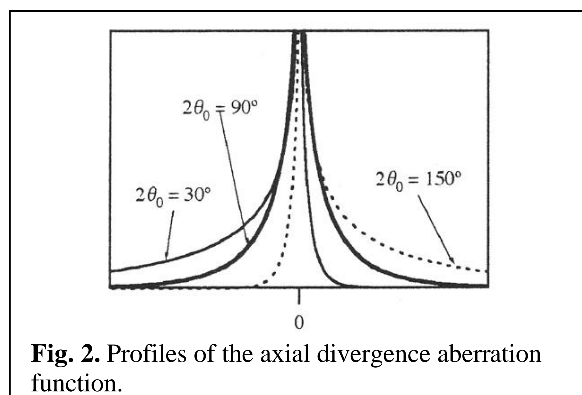


**Fig. 2.** Profiles of the axial divergence aberration function.

The FWHM $\Phi_v$ for the axial divergence is close to the open angle of the Soller slits, but it seems better to be optimized by profile fitting procedures to the intensity data of diffraction peaks collected for standard materials [7]. Once the value of $\Phi_v$ is optimized, it can be treated as a constant parameter specific to the instrument, as far as the Soller slits are fixed to the diffractometer.

As the models for axial divergence proposed by Howard [16] and van Laar *et al.* [17] neglects the divergence of the source beam, they cannot be used for Bragg-Brentano type diffractometers despite the suggestions by Finger et al. [18]. The fundamental-parameters approach to the data collected with focal geometry has become validated, only after the above accurate formula of the axial divergence aberration function has been revealed.

### *3.1.4. Flat-Specimen Effect*

If the face of the specimen has the same curvature as the focal circle, the reflections from any points on the specimen face would have the same diffraction angle. The use of specimens with flat face causes an aberration, which is called the flat-specimen aberration.

The effect of flat-specimen is schematically illustrated in Fig. 3. It should be noted that the goniometer (apparent) angle $2\Theta$ and the true diffraction angle $2\theta$ are denoted by different symbols. As shown in Fig. 3, the diffraction angle is deviated to the higher angle when the reflection

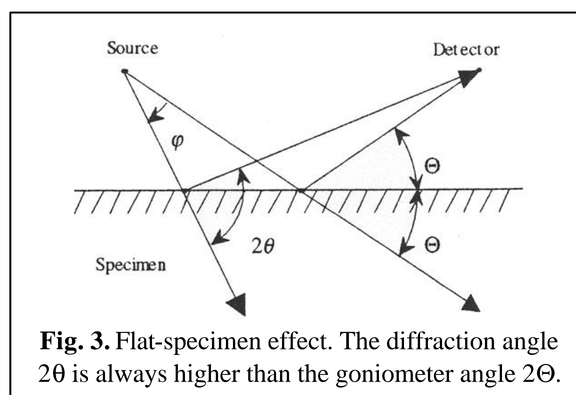


**Fig. 3.** Flat-specimen effect. The diffraction angle $2\theta$ is always higher than the goniometer angle $2\Theta$.

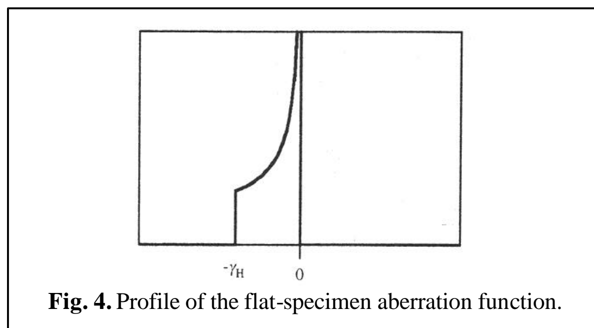


**Fig. 4.** Profile of the flat-specimen aberration function.

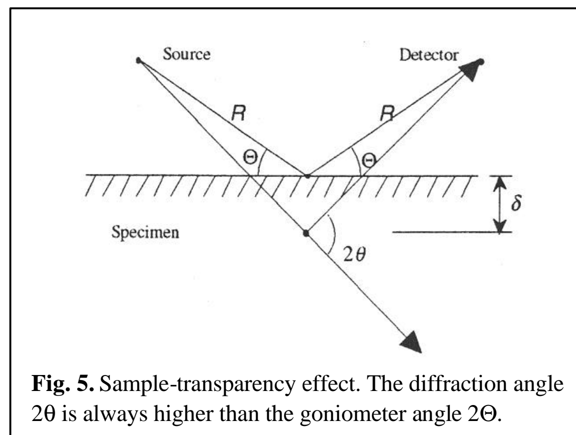


**Fig. 5.** Sample-transparency effect. The diffraction angle 2θ is always higher than the goniometer angle 2Θ.

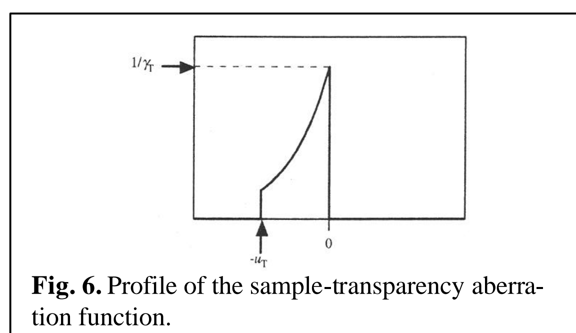


**Fig. 6.** Profile of the sample-transparency aberration function.

point is displaced from the center of the specimen. Therefore, observed peak profiles have longer tail on the lower-angle side, and the average peak position is also shifted to lower values.

The simplest model for the flat-specimen aberration function is given by

$$W_H(y;\gamma_H) = \begin{cases} 1/\sqrt{-4\gamma_H y}, & for -\gamma_H < y < 0, \\ 0, & elsewhere \end{cases} \quad (3.8)$$

$$\gamma_H = \frac{\Phi_H^2}{2\tan\theta_0} \quad (3.9)$$

where $\Phi_H$ is the open angle of the divergence/ scattering slits [3, 7].

Figure 4 shows the shape of the flat-specimen aberration function. It always shows longer tail on the lower-angle side, and it becomes more significant for the lower diffraction angles.

*3.1.5. Effect of Sample Transparency*

Although the effect of sample transparency is not significant for the samples with high absorption coefficient, the penetration of the X-ray can cause considerable aberration especially in case of organic compounds. As shown in Fig. 5, the reflection from the point deviated from the face of the specimen always takes higher diffraction angle, which causes growth of the lower angle tail in the apparent diffraction peak profile.

The sample-transparency aberration function is given by

$$W_T(u;\gamma_T,u_T) = \begin{cases} \gamma_T^{-1}\exp(u/\gamma_T), & for - u_T < u < 0, \\ 0, & elsewhere \end{cases} \quad (3.10)$$

$$\gamma_T = \sin 2\theta_0 / 2\mu R, \quad (3.11)$$

$$u_T = w_T \cos\theta_0 / R \quad (3.12)$$

where $\mu$ is the linear absorption coefficient and T the thickness of the sample [5].

It should be noted that the function is not generally normalized except the case when the thickness of the specimen can be treated as infinity. As the reduced reflection intensity of a thin sample with high transparency is taken into account in the above formula, the change of intensity caused by the finite thickness of the sample can be automatically corrected by applying a model profile function convoluted with the above aberration function.

A typical shape of the aberration function is shown in Fig. 6. It causes lower-side tail for peaks at any diffraction angles, and the maximum asymmetry occurs at the diffraction angle of 90° for an infinitely thick specimen.

### 3.2. Experimental Examination of the Instrumental Model for Focal Geometry

The validity of the instrumental model has been examined by profile fitting with the model profile function described in the preceding section to the experimentally obtained diffraction patterns. The measurement was conducted with a commercial powder X-ray diffractometer (Rigaku, RINT-2100V) with Cu Kα X-ray source and a curved graphite monochromator on the diffracted

beam side. The axial divergence angle used for analysis was 3.1°, which had been optimized by a preparatory measurement. The values of other instrumental parameters (goniometer radius, open angle of the divergence/scattering slits, width of the receiving slit) are assumed to be equivalent to those specified for the diffractometer. The temperature was kept at 299(1) K during the measurements. The standard reference material $LaB_6$ (NIST, SRM660), the lattice constant of which is 4.15695(6) A at 299 K, was used as the sample.

*3.2.1. Profiles Dependent on Divergence/Scattering Slit Angle*

The experimental diffraction peak profiles was varied by changing the divergence/scattering slit angles as $\Phi_H$=0.5, 1, 2°. Figure 7 shows the results of profile fitting by the profile function based on the fundamental-parameters approach to the experimental profiles of 111-reflection, measured with three different divergence/scattering slit angles. The fitting parameters used here are the integrated intensity, peak location and the constant background, which means that no adjustable profile parameters to fit the peak shape are used in the current profile fitting. Nonetheless, the systematic change in the profile on variation of the open angle is considerably well reproduced by the model profile function. The vertical arrows marked in Fig. 7 show the peak positions obtained by the profile fitting. The estimated peak positions are fairly well coincided, while the apparent peak-top position is considerably shifted for wide open angles of divergence/scattering slits, which supports that the intrinsic peak position unaffected by the instrumental conditions can be evaluated by this profile fitting method.

As $LaB_6$ belongs to the cubic system, the lattice constant is directly calculated from the position of each diffraction peak $2\theta_{hkl}$ as follows,

$$aobs = \frac{\lambda\sqrt{h^2+k^2+l^2}}{2\sin\theta_{hkl}} \tag{3.13}$$

Figure 8 plots the apparent lattice constant $a_{obs}$ for 24 diffraction peaks, 100 to 511/333-reflections.

The apparent lattice constant $a_{obs}$ clearly shows systematic dependence on the diffraction angle, while it should be constant if the measurement were conducted on an ideal condition. The dependence can be explained by the effects of the zero-offset error in the goniometer angle and the

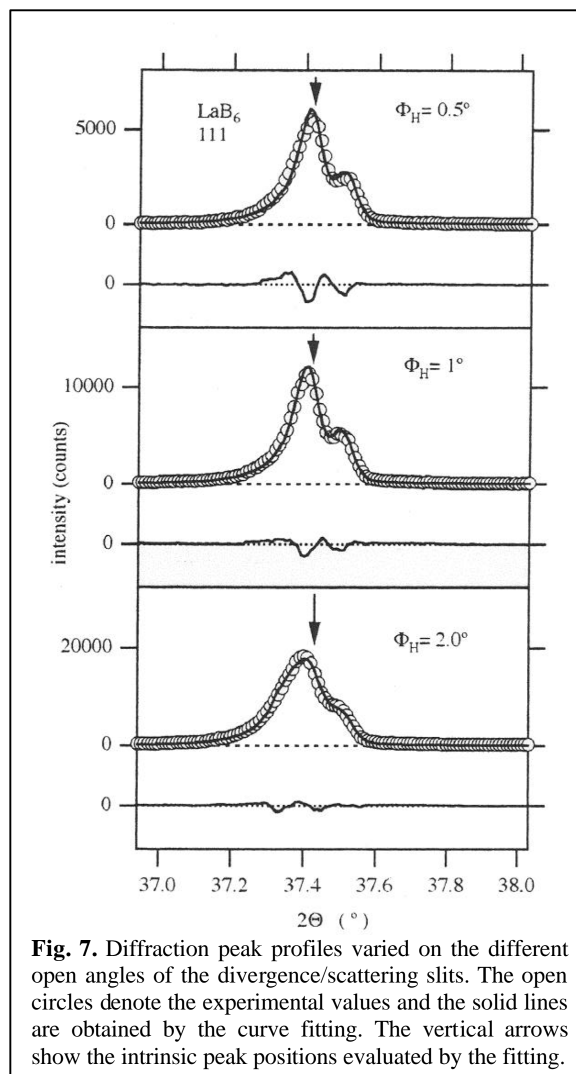


**Fig. 7.** Diffraction peak profiles varied on the different open angles of the divergence/scattering slits. The open circles denote the experimental values and the solid lines are obtained by the curve fitting. The vertical arrows show the intrinsic peak positions evaluated by the fitting.

sample displacement from the goniometer center. The peak shift for the offset error of $\Delta 2\Theta_0$ and the sample displacement of S is given by

$$\Delta 2\theta = \Delta 2\theta_0 - \frac{2S\cos\theta_0}{R} \tag{3.14}$$

Therefore, the following relation is derived:

$$a_{obs} = \frac{a\sin\left(\theta_0 - \frac{\Delta 2\Theta_0}{2} + \frac{S\cos\theta_0}{R}\right)}{\sin\theta_0} \tag{3.15}$$

where a is the true lattice constant of the sample. The results of least squares fitting with variable fitting parameters of the zero-offset error $\Delta 2\Theta_0$, sample displacement S and the true lattice constant a, are shown as solid lines in Fig. 8. As is seen in Fig. 8, the model fairly well reproduces the observed dependence of $a_{obs}$. The estimated

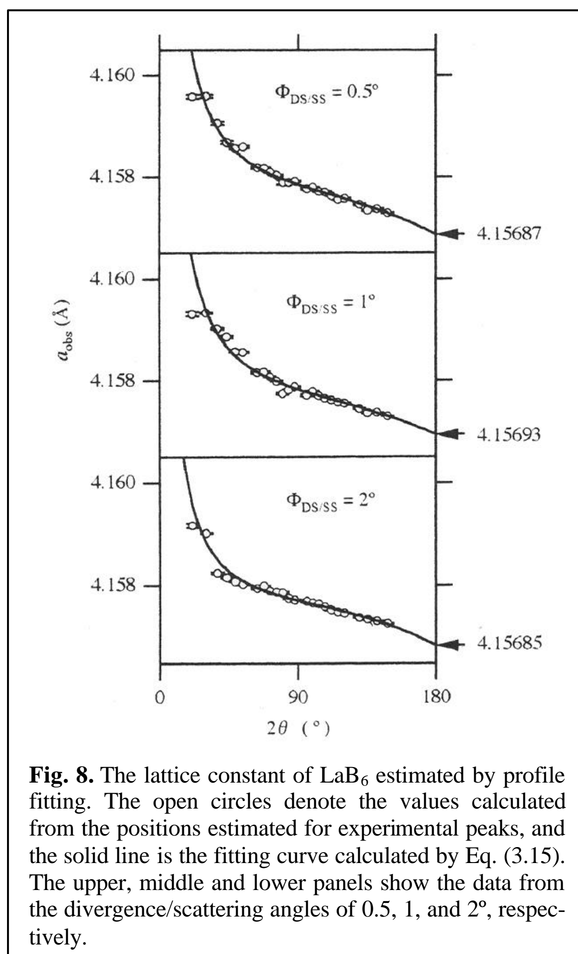


**Fig. 8.** The lattice constant of $LaB_6$ estimated by profile fitting. The open circles denote the values calculated from the positions estimated for experimental peaks, and the solid line is the fitting curve calculated by Eq. (3.15). The upper, middle and lower panels show the data from the divergence/scattering angles of 0.5, 1, and 2°, respectively.

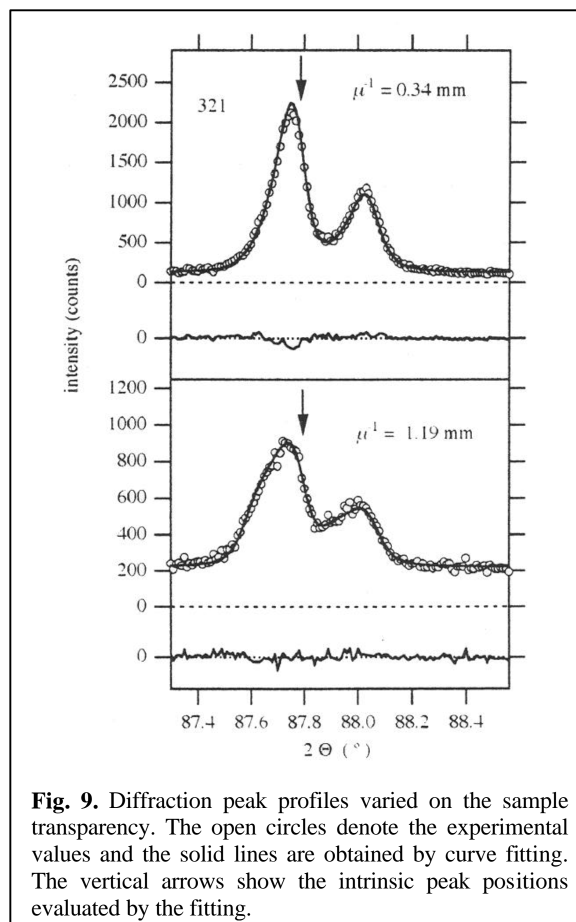


**Fig. 9.** Diffraction peak profiles varied on the sample transparency. The open circles denote the experimental values and the solid lines are obtained by curve fitting. The vertical arrows show the intrinsic peak positions evaluated by the fitting.

lattice constants are 4.15687(2), 4.15685(1) and 4.15695(1) Å for the three different measurements, which are all coincided with the specified value of 4.15695(6) Å, when the error of temperature control and thermal expansion of the material are taken into account. The values of the zero-offset error and sample displacement estimated at about $\Delta 2\Theta_0$=-0.05° and S=-0.05 mm are also reasonable. It should be emphasized that such a precise value of lattice constant has been determined without any use of standard materials.

*3.2.2. Profiles Dependent on Sample Transparency*

In order to clarify the change in the experimental peak profile varied on the sample transparency, samples of diluted $LaB_6$ were prepared as follows [5]. The $LaB_6$ powder was mixed with soluble starch ($C_6H_{10}O_5$; Wako Pure Chemical) and 2~3 ml of water with a mortar and a pestle. The mixtures were freeze-dried and ground again, and the obtained bulky (~0.5 g cm$^{-3}$) powder was used for measurement. The linear absorption coefficient of the $La_6$/starch mixture has been estimated from the mixing ratio and the apparent density of the powder sample.

Figure 9 shows the results of profile fitting for the 321-reflection peaks of two different samples with the penetration depth (the inverse of the linear absorption coefficient) of $\mu^{-1}$=0.34 and 1.19 mm, which are similar to or larger than the sample thickness of 0.5 mm.

The calculated profiles fairly well reproduce the change in the experimental profiles, which show the heavier distortion of the profile for the higher transparency and also considerable shift of the apparent peak position. No systematic trend has been left in the difference plot for the sample with the penetration depth of 1.19 mm, which means that the experimental profile has been perfectly simulated by *a priori* calculation, and the profile fitting has extracted all the information

(intensity, position and background) involved in the experimental profile.

The lattice constants, evaluated by the same way as in the preceding section, 4.15709(12) and 4.15702(7) Å for the sample of $\mu^{-1}$ =0.34 and 1.19 mm, respectively, are both coincided with the specified value within the experimental errors.

## 4. Profile Function for High-Resolution Synchrotron X-ray Powder Diffractometers

### 4.1. Model Function

It can be expected that most of optical aberrations, flat-specimen, sample transparency and displacement, are removed by use of synchrotron radiation with negligible beam divergence. The axial divergence of the diffracted beam cannot be neglected even in the case of synchrotron X-ray source, but it is easier to be modeled than the focal geometry, where divergence of both incident and diffracted beams should be simultaneously taken into account.

As shown in Fig. 10, a high-resolution synchrotron X-ray diffractometer is usually attached with a crystal analyzer and Soller slits on the diffracted beam side. Hastings et al. have tried to derive a model profile function for such geometry [19], but it does not seem to be successful, because some confusion is found in their treatment of transparency function for the Soller slits and the normalization factor of the profile function. Although Finger et al. have suggested that the model proposed by van Laar & Yelon for neutron diffractometry is also applicable to the synchrotron diffractometry [18], it is hard to justify such an overextended application to the clearly different geometry of the optics. The high correlation within the fitting parameters, frequently given by the method of Finger *et al.,* also discourages application of their method to synchrotron data.

Furthermore, as it has been known that the observed profile is sensitively deformed by slight deviation of the normal direction of the crystal analyzer from the equatorial plane, a model capable of simulating such a behavior is strongly required for practical use.

Then, we have derived practical mathematical models for instrumental functions and peak profile function, including the effects of slight misalignment of the crystal analyzer, the detail of which is

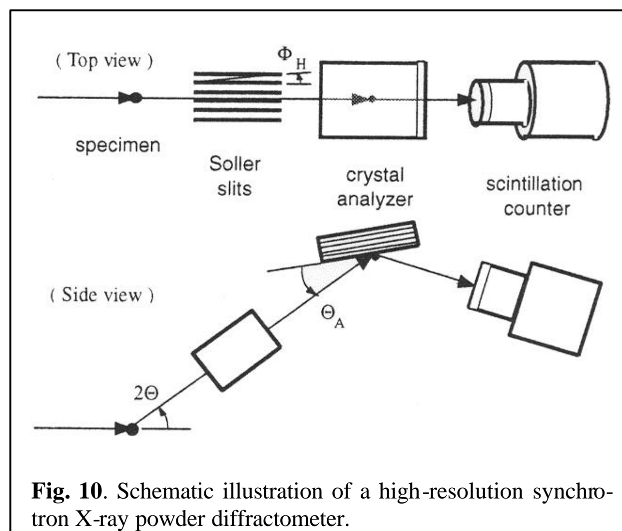


**Fig. 10**. Schematic illustration of a high-resolution synchrotron X-ray powder diffractometer.

given in Ref. [20]. In the current article, a simple formula for the profile model function synthesized by the convolution of Lorentzian function with the instrumental function for the diffractometric optics with a well-aligned analyzer is briefly presented.

#### *4.1.1. Instrumental Function for High-Resolution Synchrotron X-ray Powder Diffractometers*

When the crystal analyzer is well adjusted, and the effect of the deviation of the normal direction of the analyzer face from the equatorial direction is negligible, the instrumental function is well approximated by the following simple formula:

$$w_A(x) = \begin{cases} \dfrac{1}{|\gamma_A|}\left[\left(\dfrac{x}{\gamma_A}\right)^{-1/2} - 1\right] & for\, 0 < x/\gamma_A < 1, \\ 0 & elsewhere \end{cases} \tag{4.1}$$

$$\gamma_A \equiv -\frac{\Phi_H^2}{2}\left(\cot 2\theta + \tan\Theta_A\right) \tag{4.2}$$

where $\Phi_H$ is the open angle of the Soller slits, $2\theta$ the diffraction angle, and $\Theta_A$ the analyzer reflection angle. Note that all of the parameters have clear physical meanings in the above expression.

Figure 11 shows the shape of the instrumental function. As can be known from Eq. (4.2), the instrumental function shows lower angle tail for the diffraction angle: $2\theta < \pi/2 + \Theta_A$, and higher angle tail for the diffraction angle: $2\theta > \pi/2 + \Theta_A$.

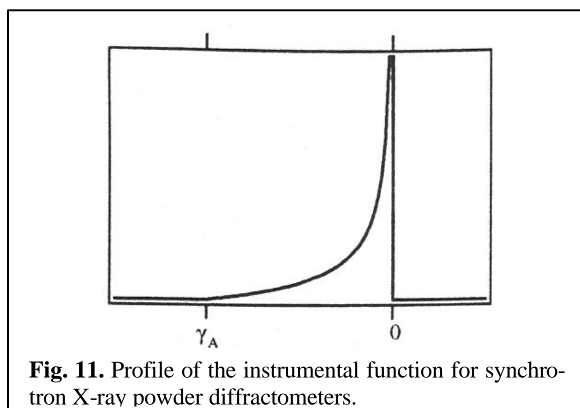


**Fig. 11.** Profile of the instrumental function for synchrotron X-ray powder diffractometers.

*4.1.2. Peak Profile Model*

The model for the diffraction peak profile is derived by the convolution of any functions with the instrumental function, which can generally be evaluated by numerical integral. The convolution of the Lorentzian function with the instrumental function given in the Section 4.1.1 can be expressed by the analytical solution represented by a combination of elementary functions. The analytical solution is expressed by the following equations,

$$p(x;\gamma_L,\gamma_A)=\frac{1}{\gamma_L}f_{LA}\left(\frac{x}{\gamma_L},\frac{\gamma_A}{\gamma_L}\right)$$

$$\begin{aligned}f_{LA}(u,v)=&\frac{1}{2\pi wp}\ln\frac{v+p+w}{v-p+w}\\&+\frac{1}{\pi wq}\left(\frac{\pi}{2}-\arctan\frac{w-v}{q}\right)\\&-\frac{1}{\pi v}\left[\frac{\pi}{2}-\arctan\left(\frac{1+u^2}{v}-u\right)\right]\end{aligned}$$

$$\text{for } v>0$$

$$f_{LA}(u,v)=f_{LA}(-u,-v)$$

$$w\equiv\sqrt{u^2+1},\ p\equiv\sqrt{2v(w+u)},q\equiv\sqrt{2v(w-u)}$$

As the above formulae only include three square roots, one logarithm and two arctangent functions, the evaluation can be quite rapid as well as the partial derivatives by parameters are easily obtained, if necessary.

## 4.2. Experimental Validation of the Instrumental Function for High-Resolution Synchrotron X-ray Powder Diffractometers

The validity of the model peak profile function given in the preceding section has been examined by profile fitting procedures to the experimental peak profiles. The diffraction data of standard silicon powder (NIST SRM 640b) were collected with a high-resolution powder X-ray diffractometer MDS [21] on the beamline BL4B2 at the Photon Factory in Tsukuba. The Soller slits limiting the axial divergence to be $\phi_H$=1° and Ge(111) flat crystal analyzer, the Bragg angle of which is $\Theta_A$=6.2° for the wavelength λ.=0.707 Å, were located on the diffracted beam side.

The 111, 220 and 311-reflections of Si were simultaneously fitted with the sum of the model functions. The instrumental parameters, the axial divergence angle and the Bragg angle of the analyzer, were treated as fixed parameters. The independent variable parameters for the fitting were the locations, intensities, Lorentzian widths and background parameters, that is, it is virtually equivalent to the simple fitting with the sum of the Lorentzian functions.

The results of the fitting are shown in Fig. 12. Although the experimental peak profile is significantly different from the Lorentzian profile, the convoluted profile function quite well reproduces the observed profiles. The R-factors for the profile fitting, $R_{wp}$=2.2%, $R_p$=1.5%, are quite small values, and systematic deviation of the model profile is hardly detectable in the difference plot.

The good coincidence between the observed and calculated profiles suggests that the intrinsic peak profile is close to the Lorentzian profile. However, the effects of spectral width and/or the slight divergence of the source X-ray may be included in this Lorentzian component. Although the model function is considered to be valid for the evaluation of intensities and positions of the diffraction peaks, a precise model for monochromating optics is needed for further detailed discussions about the line width.

## 5. Conclusions

Practical model functions for diffraction peak profiles expressed by the multiple convolutions with the valid instrumental functions, applicable to the most frequently used focal (Bragg-Brentano

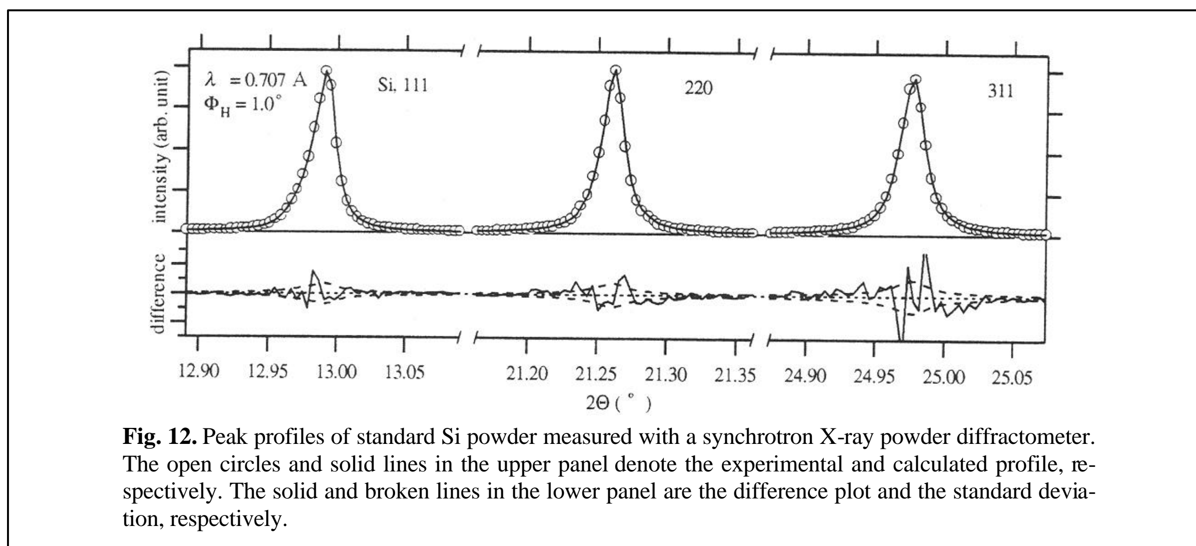

**Fig. 12.** Peak profiles of standard Si powder measured with a synchrotron X-ray powder diffractometer. The open circles and solid lines in the upper panel denote the experimental and calculated profile, respectively. The solid and broken lines in the lower panel are the difference plot and the standard deviation, respectively.

type) geometry [4, 5, 7], and to high-resolution synchrotron X-ray powder diffractometers [20], are proposed. The convoluted model of the profile function is not only preferable for the loss of theoretical ambiguity compared with the empirical model functions, but is also practically convenient because it enables automatic correction of aberrations caused by the instruments. It is expected that these functions will be widely utilized for profile analysis, decomposition of overlapped peaks and Rietveld refinement.

## References

[ 1] H. M. Rietveld, *J. Appl. Cryst.* **2**, 65-71 (1969).
[2] P. Gallezot, *Catalysis, Science and Technology*, Vol. 5, Springer-Verlag (1983).
[3] R. W. Cheary and A. A. Coelho, *J. Appl. Cryst.* **25**, 109-121 (1992).
[4] T. Ida, *Rev. Sci. Instrum*. **69**, 3837-3839 (1998).
[5] T. Ida and K. Kimura, *J. Appl. Cryst.* **32**, 982-991 (1999)
[6] G. Hölzer, M. Fritsh, M. Deutsch, J. Hartwig, and E. Forster, *Phys. Rev. A* **56**, 4554 (1997).
[7] T. Ida and K. Kimura, *J. Appl. Cryst.* **32**, 634-640 (1999).
[8] A. H. Compton and S. K. Allison, *X-Rays in Theory and Experiment*, pp. 740-750. New York; D. VAN NOSTRAND (1935).
[9] F. Schreier, *J. Quant. Spectrosc. Radiat. Transfer* **48**, 743-762 (1992).
[10] G. P. M. Poppe and C. M. J. Wijers, *ACM Trans. Math. Software* **16,** 38 (1990); http://www.acm.org/pubs/ citations/journals/ toms/1990-16-1/p47-poppe/
[11] G. K. Wertheim, *Rev. Sci. Instrum.* **45**, 1369-1371 (1974).
[12] P. Thompson, D. E. Cox and J. B. Hastings, *J. Appl. Cryst*. **20**, 79 (1987).
[13] T. Ida, M. Ando, and H. Toraya, *J. Appl. Cryst.* **33**, 1311 (2000).
[14] T. Ida, *Rev. Sci. Instrum.* **69**, 2268-2272 (1998).
[15] W. H. Press, B. P. Flannery, S. A. Teukolsky, and W. T. Vetterling, *Numerical Recipes*, Cambridge Univ. Press (1986).; http://www.nr.com
[16] C. J. Howard, *J. Appl. Cryst.* 1**5**, 615-620 (1982).
[17] B. van Laar and W. B. Yelon, *J. Appl. Cryst.* **17**, 47-54 (1984).
[18] L. W. Finger, D. E. Cox and A. P. Jephcoat, *J. Appl. Cryst.* **27**, 892-900 (1994).
[19] J. B. Hastings, W. Thomlinson and D. E. Cox, *J. Appl. Cryst.* **17**, 85-95 (1984).
[20] T. Ida, H. Hibino and H. Toraya, *J. Appl. Cryst.* **34**, 144-151 (2001).
[21] H. Toraya, H. Hibino and K. Ohsumi, *J. Synchrotron Rad.* **3**, 75-83 (1996).